





RESEARCH ARTICLE | MAY 02 2023

## The circulation growth of non-impulsive starting jet

Zhu Jianwei (朱建玮) ; Zhang Guoqing (张国庆) ; Gao Lei (高磊) ; Yu S. C. M. (余澄文) 



*Physics of Fluids* 35, 057102 (2023)

<https://doi.org/10.1063/5.0147768>



### Articles You May Be Interested In

An extended model for orifice starting jets

*Physics of Fluids* (June 2021)

Negatively buoyant starting jets

*Physics of Fluids* (November 2009)

Vortex formation in starting buoyant jets at moderate Richardson numbers

*Physics of Fluids* (November 2020)



Physics of Fluids

Special Topics Open  
for Submissions

[Learn More](#)

# The circulation growth of non-impulsive starting jet

Cite as: Phys. Fluids **35**, 057102 (2023); doi: [10.1063/5.0147768](https://doi.org/10.1063/5.0147768)

Submitted: 25 February 2023 · Accepted: 14 April 2023 ·

Published Online: 2 May 2023



View Online



Export Citation



CrossMark

Jianwei Zhu (朱建玮),<sup>1,a)</sup> Guoqing Zhang (张国庆),<sup>1,b)</sup> Lei Gao (高磊),<sup>2</sup> and S. C. M. Yu (余澄文)<sup>3</sup>

## AFFILIATIONS

<sup>1</sup>Key Laboratory of Dynamics and Control of Flight Vehicle, School of Aerospace Engineering, Beijing Institute of Technology, Beijing 100081, People's Republic of China

<sup>2</sup>School of Aeronautics and Astronautics, Sichuan University, Chengdu 610065, People's Republic of China

<sup>3</sup>Department of Aeronautical and Aviation Engineering, The Hong Kong Polytechnic University, Kowloon, Hong Kong, People's Republic of China

<sup>a)</sup>Electronic mail: [18801135578@163.com](mailto:18801135578@163.com)

<sup>b)</sup>Author to whom correspondence should be addressed: [zhanggq@bit.edu.cn](mailto:zhanggq@bit.edu.cn)

## ABSTRACT

An analytical model that can be used to predict the circulation growth process for non-impulsive starting jets has been developed by extending the over-pressure correction model for impulsive starting jets. Only the jet velocity function  $U_0(t)$  is needed to obtain the circulation growth process of non-impulsive starting jet. The non-impulsive starting jets generated by nozzle and orifice configurations are performed numerically with two acceleration schemes (represented by two kinds of velocity functions) and different acceleration stage stroke ratios  $L_a D$  (modifying the acceleration time  $t_a$  in each velocity function to obtain  $L_a D = 0.05 : 0.2 : 1.25$ ) to verify the accuracy of the proposed analytical model. The influence of radial velocity distribution in the jet inflow boundary is ignored in the process of constructing this model, but this has been proven to be reasonable. The time-averaged relative error with the growth process of the total circulation predicted by this model is about 11% to 26%, which is smaller than the 44% to 88% obtained by the classical slug model. For the range of  $L_a D$  from 0.05 to 1.25, the relative error with the prediction of the total circulation at the end of the acceleration stage is from 4% to 28%, as compared to the 39% to 96% for the slug model.

Published under an exclusive license by AIP Publishing. <https://doi.org/10.1063/5.0147768>

## I. INTRODUCTION

Starting jet is a typical unsteady flow, which can be taken as the initial stage of a steady jet or a single-pulse jet with finite discharged volume. It is an important feature of many flow systems ranging from biological propulsion<sup>1–7</sup> to flow control<sup>8,9</sup> and even the blood flow in the human heart.<sup>10</sup> The piston–cylinder mechanism combined with nozzle or orifice configuration has been widely used in the experimental study of starting jets.<sup>11–17</sup> During the initial stage of the starting jet, the boundary layer separates and rolls up at the nozzle (orifice) edge to form a vortex ring (the leading vortex ring). The vortex ring grows by absorbing vorticity and fluid from the trailing jet.<sup>11,18,19</sup> The vorticity flux across the jet inflow boundary, which is equal to the circulation growth rate of starting jet, controls the formation and evolution process of the leading vortex ring and starting jet.<sup>19,20</sup>

One of the most interesting phenomena during the formation process of the leading vortex ring is the “pinch-off.” The phenomenon of pinch-off was first observed experimentally by Gharib *et al.*<sup>11</sup>

In that study, the piston–cylinder mechanism combined with nozzle configuration was used to generate the starting jets with a wide range of piston stroke ratios and the accompanying leading vortex ring. It was observed that only a single leading vortex ring was produced when the stroke ratio was small, and a trailing jet appeared behind it with the increase in the stroke ratio to more than approximately 4. The vorticity field of the leading vortex ring then got separated from that of the trailing jet and no longer absorbed the vorticity from the trailing jet, which indicated the occurrence of pinch-off. Subsequently, a universal timescale called the “formation number” was proposed by Gharib *et al.*<sup>11</sup> to indicate the occurrence of the pinch-off phenomenon. After that, many researchers tried to establish models to predict the occurrence of pinch-off, i.e., the formation number under different cases, by kinematic or dynamic.<sup>11,14,16,21–24</sup> Since the circulation growth rate of the starting jet is one of the controlling factors for the development of the starting jet and the leading vortex ring, the establishment of all the above models required the total circulation growth rate of the starting jet to be known beforehand.

Gharib *et al.*<sup>11</sup> used the Kelvin–Benjamin variation principle<sup>25</sup> to define dimensionless energy, which can be used to predict the formation number. Mohseni and Gharib<sup>21</sup> predicted the formation number by equating the leading vortex ring to a member of the Norbury family vortex rings<sup>26,27</sup> and incorporating the Kelvin–Benjamin variation principle. Shusser *et al.*<sup>22</sup> suggested that the time when the translational velocity of the leading vortex ring exceeds the jet velocity can be used to predict the occurrence of pinch-off, which is also known as the kinematic criterion. Shusser and Gharib<sup>28</sup> demonstrated that the kinematic criterion is actually equivalent to the Kelvin–Benjamin variation principle. The slug model, which assumes the velocity at the jet inflow boundary is uniform, was used in the above three pinch-off prediction models to approximate the circulation growth rate of starting jet, i.e.,

$$\frac{d\Gamma_{total}}{dt} = \frac{1}{2} U_0^2(t), \quad (1)$$

where  $\Gamma_{total}$  is the total circulation of starting jet,  $U_0(t)$  is the average velocity of the jet at the jet inflow boundary, and  $t$  is the flow time. The slug model was first introduced by Didden<sup>19</sup> and Glezer<sup>29</sup> to predict the circulation growth rate of parallel starting jets, and it was extended by Gharib *et al.*<sup>11</sup> to predict the hydrodynamic impulse and kinetic energy. Therefore, the above three pinch-off prediction models are limited to predicting the pinch-off in the parallel starting jet (straight nozzle configuration).

To better predict the pinch-off, Shusser *et al.*<sup>30</sup> corrected the jet velocity in the kinematic criterion suggested by Shusser *et al.*<sup>22</sup> by considering the existence and development of boundary layers. Dabiri and Gharib<sup>31</sup> modified the expression and obtained

$$U_c(t) = U_0(t) \left( 1 + \frac{8}{\sqrt{\pi}} \sqrt{\frac{\gamma t}{D^2}} \right), \quad (2)$$

where  $\gamma$  is the kinematic viscosity of the fluid, and  $D$  is the diameter of nozzle. As for  $U_c(t)$ , it is the velocity of the uniform region within the nozzle excluding the boundary layer, named as core velocity. The acceleration stage of the starting jet has been taken into account, so it can be used to calculate the core velocity  $U_c(t)$  for the non-impulsive starting jet. The above equation is also used by Dabiri and Gharib<sup>31</sup> to modify the slug model to obtain the circulation growth rate of starting jet but ignoring the initial acceleration stage, i.e.,

$$\frac{d\Gamma_{total}}{dt} = \frac{1}{2} \left( 1 + \frac{8}{\sqrt{\pi}} \sqrt{\frac{\gamma t}{D^2}} \right)^2 U_0^2. \quad (3)$$

Gao and Yu<sup>23</sup> obtained a two-stage model for vortex ring formation and the pinch-off process in both straight and converging nozzles by modifying the model proposed by Shusser and Gharib<sup>32</sup> for vortex ring formation in a starting buoyant plume. The problem that the circulation growth rate of starting jet is actually higher than that of the slug model after the jet develops for a period of time has also been considered.<sup>33</sup> Gao and Yu<sup>23</sup> used the approximation of vortex flux through the jet inflow boundary from Didden,<sup>19</sup> as follows:

$$\frac{d\Gamma_{total}}{dt} = 0.57 U_0^2. \quad (4)$$

This implicitly assumes that the piston reaches a constant velocity  $U_0$  immediately after the jet is initiated.

Krieg and Mohseni<sup>14</sup> suggested a new kinematic criterion that uses the moment at which the velocity induced at the origin of the leading vortex ring exceeds the maximum feed velocity at the centerline (twice the jet velocity) as the criterion for predicting the onset of pinch-off. This criterion can be used for the starting jets generated by both the nozzle and orifice configurations. The method used to determine the circulation growth rate of starting jet is the two-dimensional model proposed by Krieg and Mohseni,<sup>13</sup> i.e.,

$$\frac{d\Gamma_{total}}{dt} = \frac{1}{2} (1 + K) U_0^2(t), \quad (5)$$

where  $K$  is the radial slope of  $\partial v \partial x$  normalized by the jet velocity and nozzle (orifice) radius,  $K = kR^2/U_0$ .  $\partial v \partial x$  is the axial gradient of radial velocity, and its radial distribution is assumed to be  $\partial v \partial x = kr$ .<sup>13</sup> The value of  $K$  is taken as a constant value by adopting the assumption of the large stroke ratio, which is equivalent to ignoring the initial acceleration stage.<sup>14</sup>

Limbourg and Nedić<sup>16</sup> used a new timescale in terms of the contracted quantities and combined three non-dimensional numbers to unify the formation number of starting jet in orifice and nozzle configurations. The circulation growth rate of starting jet was estimated by a revised slug model, i.e.,

$$\frac{d\Gamma_{total}}{dt} = \frac{1}{2} U_0^2 \times \frac{1}{C_c^2}, \quad (6)$$

where  $C_c$  is the contraction coefficient defined as the ratio of the area of *vena contracta* to the area of the orifice.<sup>34,35</sup> In addition, the straight nozzle would experience a contraction of the flow due to the existence of the boundary layer and the contraction coefficient changes from 1 to 0.9. This would match its non-dimensional energy curve well with the slug model. Therefore, the circulation growth rate of starting jet for the nozzle configuration can be expressed as

$$\frac{d\Gamma_{total}}{dt} = 0.62 U_0^2, \quad (7)$$

which is larger than that used by Gao and Yu.<sup>23</sup> Similar to the previous model, the model can only be verified with the impulsive starting jet from Limbourg and Nedić<sup>17</sup> due to the absence of considering the initial acceleration stage.

The above research works on the prediction of the vortex ring pinch-off process all require the circulation growth rate of starting jet to be known. Five methods for predicting the circulation growth rate of starting jet have been proposed, see Eqs. (1) and (3)–(6). Compared to the impulsive starting jet, the non-impulsive starting jet is closer to the actual application scene of the starting jet.<sup>2,5,7,36</sup> Recent research works have also gradually began to focus on the non-impulsive starting jets.<sup>37–39</sup> However, the above methods for calculating the circulation growth rate of starting jet only consider the impulsive starting jet and ignore the initial acceleration stage, except for Eqs. (1) and (5). However, Eq. (1) underestimated the circulation growth rate of starting jet in the acceleration stage of the parallel starting jet (nozzle configuration) and the entire process of the non-parallel starting jet (orifice configuration).<sup>13,14,19,33,35,37,40,41</sup> Krueger<sup>35</sup> made up for the deficiency by adding an added contribution term due to “overpressure” for impulsively starting jet. It is interesting to note that this model does not consider the transient process of circulation growth

and also neglects the vortex ring formation under the approximation of potential flow. Equation (5) is a semi-empirical model derived by Krieg and Mohseni,<sup>13,14</sup> and the parameter  $K$  changes drastically during the initial acceleration of the starting jet [see Fig. 14(b) in Ref. 13]. This reduces the practicability of the method in the initial acceleration stage of the non-impulsive starting jet.

Circulation growth rate is also critical for the applications of starting jet. Holman *et al.*<sup>42</sup> suggested that the rate of circulation from the synthetic jet generator to the outflow field is important for defining the formation criteria of synthetic jets. The evolution of vortex structure in the jet wake, which is also influenced by the circulation growth rate, can affect the performance of pulsed jet propulsion.<sup>5,6</sup> However, the starting jets generated by the synthetic jet generator and pulsed jet propulsion are pulsed jets with finite discharged volume, and their stroke ratios are not large enough to ignore the initial acceleration stage.<sup>2,42,43</sup> In addition, it was found that the circulation growth rate of starting jet is critical to the formation of the vortex ring in the starting forced plumes (starting jet with buoyancy effect).<sup>44–47</sup> The buoyancy affects the formation of the vortex ring by changing the circulation growth rate of the starting jet. Therefore, it is necessary to study the mechanism for the circulation growth of the starting jet to provide a better circulation prediction method considering the initial acceleration stage.

In the present work, we present a model to calculate the circulation growth rate of non-impulsive starting jets with initial acceleration stage for nozzle and orifice configurations by extending the over-pressure correction model for impulsive starting jets. To verify the accuracy and availability of this model, the results predicted by this model and also from the numerical simulation are compared for the non-impulsive starting jet with two acceleration schemes (represented by two kinds of velocity functions) and different acceleration stage stroke ratios (modifying the acceleration time in each velocity function to obtain  $L_a/D = 0.05 : 0.2 : 1.25$ ).

The paper is organized as follows: The analysis of the mechanism for the circulation growth of non-impulsive starting jets and the derivation of extending the over-pressure correction model to obtain the model for calculating the circulation growth rate of non-impulsive starting jets, which considers the initial acceleration stage, are given in Sec. II. Section III introduces and verifies the numerical method that will be used to test the performance of this model. In Sec. IV, the results obtained by the numerical method are compared with that obtained by the extended pressure-correction model. In the remaining part of Sec. IV, the error source of the model will be analyzed and the model will be modified to improve the accuracy. The paper ends with brief concluding remarks in Sec. V.

## II. THE EXTENDED OVER-PRESSURE CORRECTION MODEL

Starting from the vorticity transport equation, Krueger<sup>35</sup> obtained the total circulation of the starting jet generated by the nozzle and orifice configurations as

$$\Gamma_{total}(t) = \frac{1}{2} \int_0^t u_{cl}^2(t) dt + \frac{1}{\rho} \int_0^t P_{cl}(t) dt - \int_0^{R_\infty} v(t, r)|_{x=0} dr, \quad (8)$$

where  $u_{cl}$  and  $P_{cl}$  are the axial velocity and gauge pressure at the center of the jet inflow boundary, respectively,  $v(t, r)|_{x=0}$  is the radial velocity distribution in the jet inflow boundary, and  $R_\infty$  represents the position

of radial infinity. Differentiating the above equation with respect to time can obtain the circulation growth rate,

$$\frac{d\Gamma_{total}}{dt} = \frac{1}{2} u_{cl}^2(t) + \frac{P_{cl}(t)}{\rho} - \frac{\partial}{\partial t} \int_0^{R_\infty} v(t, r)|_{x=0} dr. \quad (9)$$

The first term on the right-hand side is a vorticity flux term, which is denoted as  $d\Gamma_u/dt$ ; the second term on the right-hand side is generated by the over-pressure in the jet inflow boundary and is denoted as  $d\Gamma_p/dt$ ; the third item on the right-hand side is caused by the change of radial velocity distribution in the jet inflow boundary, denoted as  $d\Gamma_{dv/dt}/dt$ . From the pressure distribution equation in the jet inflow boundary [see Eq. (2.23) in Ref. 13], we can obtain

$$\frac{P_{cl}(t)}{\rho} = \int_0^{R_\infty} \left[ u(t, r)|_{x=0} \frac{\partial v(t, r)|_{x=0}}{\partial x} + \frac{\partial v(t, r)|_{x=0}}{\partial t} \right] dr - \frac{1}{2} v_{cl}^2, \quad (10)$$

where  $u(t, r)|_{x=0}$  is the axial velocity distribution in the jet inflow boundary, and  $v_{cl}$  is the radial velocity at the center of the jet inflow boundary. Based on the axisymmetric assumption of the flow,  $v_{cl} = 0$ . Therefore, Eq. (10) can be rewritten as

$$\frac{P_{cl}(t)}{\rho} = \int_0^{R_\infty} u(t, r)|_{x=0} \frac{\partial v(t, r)|_{x=0}}{\partial x} dr + \frac{\partial}{\partial t} \int_0^{R_\infty} v(t, r)|_{x=0} dr. \quad (11)$$

Substituting Eq. (11) in Eq. (9), we can obtain

$$\frac{d\Gamma_{total}}{dt} = \frac{1}{2} u_{cl}^2(t) + \int_0^{R_\infty} u(t, r)|_{x=0} \frac{\partial v(t, r)|_{x=0}}{\partial x} dr. \quad (12)$$

This is the equation for calculating the vorticity flux through the jet inflow boundary, equivalent to the circulation growth rate.<sup>13,14,48,49</sup>

When only the final total circulation is considered, the upper limit of the integral in Eq. (8) should be infinity. This can be equivalent to the situation after the jet is stopped for a single-pulse jet, so that  $v(t, r)|_{x=0} = 0$ . The third term on the right-hand side of Eq. (8) is, therefore, ignored by Krueger.<sup>35</sup> We could also assume that the variation of the radial velocity distribution at the jet inflow boundary has little effect on the circulation growth process of non-impulsive starting jet, so that Eq. (8) becomes

$$\Gamma_{total} = \Gamma_u + \Gamma_p, \quad (13)$$

where

$$\Gamma_u = \frac{1}{2} \int_0^t u_{cl}^2(t) dt, \quad (14)$$

$$\Gamma_p = \frac{1}{\rho} \int_0^t P_{cl}(t) dt. \quad (15)$$

By using the assumption that the front of material surface for starting jet is close to flat owing to the rapid flow initiation,<sup>50</sup> Eq. (15) can be approximated by

$$\Gamma_p = \frac{U_{0max} D}{C_p}, \quad (16)$$

where  $C_p = \pi$  for the nozzle configuration,  $C_p = 2$  for the orifice configuration, and  $U_{0max}$  is the maximum value of jet velocity. It should be noted that the assumption used to obtain Eq. (16) is only applicable

when the stroke ratio in the initial acceleration stage is far less than 1.<sup>35</sup> However, the applicability of the generalized form of this equation when the stroke ratio in the initial acceleration stage is close to 1 or even greater than 1 will be verified in the present work. Therefore, Eq. (13) is modified to become

$$\Gamma_{total} = \frac{1}{2} \int_0^t u_{cl}^2(t) dt + \frac{U_{0max} D}{C_p}. \quad (17)$$

For the case that the velocity program is a monotonic continuous function, that is, the initial acceleration stage of starting jet, the above equation can be further modified as

$$\Gamma_{total}(t) = \frac{1}{2} \int_0^t u_{cl}^2(t) dt + \frac{\int_0^t a(t) dt D}{C_p}, \quad (18)$$

where  $a(t)$  is the acceleration of the jet velocity  $U_0$ . By differentiating the above equation against time  $t$ , we can obtain

$$\frac{d\Gamma_{total}}{dt} = \frac{1}{2} u_{cl}^2(t) + \frac{a(t) D}{C_p}. \quad (19)$$

Comparing with Eq. (9), the circulation growth rate calculated by Eq. (19) lacks  $d\Gamma_{dv}/dt$  and the circulation growth caused by the over-pressure in the jet inflow boundary can be calculated directly by the jet velocity  $U_0(t)$  as

$$\frac{d\Gamma_p}{dt} = \frac{a(t) D}{C_p}, \quad (20)$$

and the flux term can be expressed as

$$\frac{d\Gamma_u}{dt} = \frac{1}{2} u_{cl}^2(t). \quad (21)$$

The key to modeling the flux term is to obtain the axial velocity at the center of the jet inflow boundary  $u_{cl}$  from the jet velocity  $U_0(t)$ . Krueger<sup>35</sup> obtained a method that can calculate the  $u_{cl}$  for the impulsive starting jets in nozzle and orifice configurations. Motivated by the model for  $d\Gamma_p/dt$  [see Eq. (20)], we can also generalize the method for predicting  $u_{cl}$  in impulsive starting jet obtained by Krueger<sup>35</sup> to the non-impulsive starting jet with the acceleration stage.

For the nozzle configuration,  $u_{cl}$  can be calculated by

$$u_{cl}(t) = \frac{U_c(t)}{1 + 0.595(1 - \sigma_n(t))}, \quad (22)$$

where  $U_c(t)$  is the core velocity and can be calculated by Eq. (2) based on jet velocity  $U_0(t)$  for short acceleration periods (stroke ratio less than 10).  $\sigma_n(t)$  is a transition function. Based on the fact that the velocity of the leading vortex ring moving away from the jet inflow boundary gradually increases and finally stabilizes,<sup>19</sup>  $\sigma_n(t)$  can be written as

$$\sigma_n(t) = \begin{cases} \frac{U_{tr}(t)}{U_0/2}, & U_{tr}(t) < U_0/2, \\ 1, & U_{tr}(t) \geq U_0/2, \end{cases} \quad (23)$$

where  $U_{tr}(t)$  represents the translational velocity of vortex ring, and the critical value  $U_0/2$  is obtained by Mohseni and Gharib<sup>21</sup> using the

slug model. Didden<sup>19</sup> experimentally measured  $U_{tr}(t)$  as  $0.42 U_0 \sqrt{L(t)/D}$ , where  $L(t)/D$  is the piston stroke ratio (equivalent to  $t^*$ ). Considering that the jet velocity varies with time,  $0.42 U_0 \sqrt{L(t)/D}$  can be rewritten as  $0.42 U_0(t) \sqrt{L(t)/D}$ . Equation (23) can, then, be rewritten as

$$\sigma_n(t) = \begin{cases} 0.84 \sqrt{L(t)/D}, & L(t)/D < 1.42, \\ 1, & L(t)/D \geq 1.42. \end{cases} \quad (24)$$

For the orifice configuration,  $u_{cl}$  can be calculated by

$$u_{cl}(t) = \frac{U_0(t)}{2 + \sigma_n(t)(C_c - 2)}, \quad (25)$$

where  $C_c$  is the contraction coefficient,<sup>34</sup> and the method to calculate it has been summarized in Limbourg and Nedić.<sup>15</sup> Continuing the method of calculating  $\sigma_n$  from Krueger<sup>35</sup> and considering the jet velocity varying with time when calculating stroke ratio  $L(t)/D$ , the equation for calculating  $\sigma_n(t)$  in the orifice configuration becomes

$$\sigma_n(t) = \begin{cases} \frac{0.84}{C_c^{0.75}} \sqrt{L(t)/D}, & L(t)/D < 1.42 C_c^{1.5}, \\ 1, & L(t)/D \geq 1.42 C_c^{1.5}. \end{cases} \quad (26)$$

In addition, Krueger<sup>35</sup> introduced  $P_{cl} > 0$  at the center of the inflow boundary caused by flow contraction into  $u_{cl}$  according to the Bernoulli equation, that is,  $u_{cl}$  at *vena contracta* was used to replace that at the jet inflow boundary.

We have obtained a model (named as OP model in the following), see Eq. (19), that can calculate the circulation growth rate of the non-impulsive starting jet according to the jet velocity  $U_0(t)$  by extending the over-pressure correction model for the impulsive starting jet from Krueger,<sup>35</sup> which does not take into account the acceleration process of the starting jet.  $u_{cl}$  in Eq. (19) can be calculated by Eq. (22) in the nozzle configuration and by Eq. (25) in the orifice configuration, and  $a(t)$  in Eq. (19) can be obtained by differentiating the jet velocity  $U_0(t)$  with respect to time  $t$ .

### III. NUMERICAL METHOD AND VERIFICATION

To verify the accuracy of this model, the numerical method will be used to simulate the non-impulsive starting jet generated by the nozzle and orifice configurations with two acceleration schemes (represented by two kinds of velocity functions) and different acceleration stage stroke ratios (modifying the acceleration time in each kind velocity function). Computational domain and boundary conditions for nozzle and orifice configurations are shown in Fig. 1. To improve the calculation efficiency and shorten simulation time, the two-dimensional numerical simulation would be used based on the axisymmetric assumption of starting jet.<sup>14,15,17</sup> The size of the computational domain is  $14D$  below the jet inflow boundary ( $x = 0, 0 \leq r \leq 0.5D$ ) in the axial direction and  $5D$  in the radial direction, where  $D$  is the diameter of the jet inflow boundary to form the starting jet. The study of Gao and Yu<sup>46</sup> and Gao *et al.*<sup>38</sup> showed that this size of the computational domain would be large enough so that the outer boundary conditions have no influence on the development of starting jet. The domain independence test has also been performed, and the parameters used and results are summarized in Table I. The cases tested in the present work are shown in Table II. The total circulation of starting jet



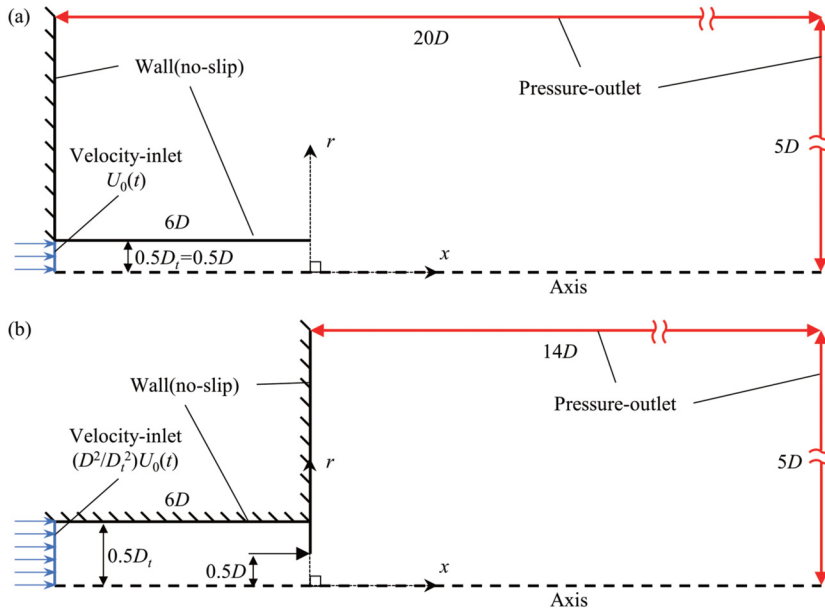


**FIG. 1.** Computational domain and boundary conditions for nozzle (a) and orifice (b) configurations, where  $D$  is the diameter of the jet inflow boundary to form the starting jet, and  $D_i$  is the diameter of the tube.

at  $t^* = 3.9715$  in the nozzle and orifice configurations hardly differs (far less than 1%) between the two largest domains. The computational domain  $14D \times 5D$  can, therefore, be considered sufficiently large. The length of the tube generating jet is  $6D$  to ensure the parallel flow in the tube before ejection.<sup>13,14</sup> To simulate the movement of the piston, the fluid enters by the velocity inlet on the left side of the tube ( $x = -6D$  and  $0 \leq r \leq 0.5D_i$ , where  $D_i$  is the diameter of the tube) with a special velocity program.<sup>48</sup> The wall forming the nozzle and orifice configurations would adopt the non-slip condition. For the outlet boundary conditions, the pressure-outlet condition is applied.

We define the jet velocity  $U_0(t)$  as the average velocity at the jet inflow boundary ( $x = 0$ ,  $0 \leq r \leq 0.5D$ ). This definition is independent of the configuration used to generate the jet. Based on the incompressible continuity equation, the velocity at the velocity inlet is equal to  $U_0(t)$  for the nozzle configuration and  $(D^2/D_i^2)U_0(t)$  for the orifice configuration. The function form of the velocity program for two acceleration schemes is given by

**TABLE I.** Summary of the parameters and results for the domain independence test.  $X$  is the axial computational domain size below the jet inflow boundary, and  $R$  is the radial direction. The relative error is calculated by taking the maximum domain as the accurate value.

Configuration	Domain size ( $X \times R$ )	$\Gamma(t^* = 3.9715)$ ( $\text{cm}^2/\text{s}$ )	Relative error (%)
Nozzle (case 3)	$7D \times 2.5D$	56.143 41	0.063 96
	$14D \times 5D$	56.178 00	0.002 39
	$21D \times 7.5D$	56.179 34	...
Orifice (case 17)	$7D \times 2.5D$	108.228 83	0.012 72
	$14D \times 5D$	108.249 30	0.006 19
	$21D \times 7.5D$	108.242 60	...

$$\frac{U_0(t)}{U_{0\max}} = \begin{cases} \sin\left(\frac{\pi}{2} \times \frac{t}{t_a}\right), & t \leq t_a, \\ 1, & t > t_a, \end{cases} \quad (27)$$

and

$$\frac{U_0(t)}{U_{0\max}} = \begin{cases} \frac{t}{t_a} - \frac{1}{2\pi} \sin\left(2\pi \times \frac{t}{t_a}\right), & t \leq t_a, \\ 1, & t > t_a, \end{cases} \quad (28)$$

where  $t_a$  is the duration of the acceleration stage (different  $t_a$  corresponding to different acceleration stage stroke ratios) and  $U_{0\max} = 0.1 \text{ m/s}$ . The acceleration schemes defined by Eqs. (27) and (28) are denoted as SIN and SIN2, respectively. The acceleration stage stroke ratio is defined as

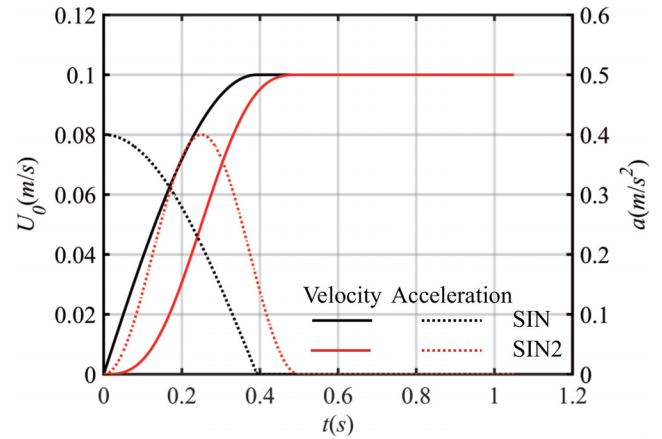
$$L_a/D = \frac{\int_0^{t_a} U_0(t) dt}{D}. \quad (29)$$

The jet velocity  $U_0(t)$  and acceleration  $a(t)$  corresponding to the acceleration schemes SIN and SIN2 are shown in Fig. 2 for  $L_a/D = 1.25$ . It can be seen that the acceleration of SIN is the largest at the beginning and then gradually decreases to 0 at  $t = 0.3927 \text{ s}$ , while the acceleration of SIN2 first rises to the peak from 0 at the beginning and then decreases to 0 at  $t = 0.5 \text{ s}$ . In Krueger's analysis, an upper limit on the validity of the acceleration stage stroke ratio ( $L_a/D \ll 1$ ) was imposed on the application scope of the over-pressure correction model based on the assumption of the impulsively starting jet.<sup>35</sup> The present work extends this model to the non-impulsive starting jet and focuses on its transient calculation accuracy in the initial acceleration stage. Therefore, it will be verified whether the extended pressure-correction model (OP model) is applicable for the acceleration stage stroke ratio  $L_a/D$  ranging from 0.05 (far less than 1) to 1.25 (greater than 1).

**TABLE II.** Summary of flow parameters for the starting jet with different configurations, acceleration schemes, and acceleration stage stroke ratios ( $L_a/D$  and  $t_a$ ).

Case	$D$ (mm)	$D_t$ (mm)	Configuration	Acceleration scheme	$L_a/D$	$t_a$ (s)
1	18.2	18.2	Nozzle	Line (0.050 to 0.147 m/s)	6.33	1.168 7
2	19.6	21.6	Orifice	Line (0.021 to 0.082 m/s)	5.53	2.103 4
3	20	20	Nozzle	SIN	0.05	0.015 7
4					0.25	0.078 5
5					0.45	0.141 4
6					0.65	0.204 2
7					0.85	0.267 0
8					1.05	0.329 9
9					1.25	0.392 7
10				SIN2	0.05	0.02
11					0.25	0.10
12					0.45	0.18
13					0.65	0.26
14					0.85	0.34
15					1.05	0.42
16					1.25	0.50
17	20	40	Orifice	SIN	0.05	0.015 7
18					0.25	0.078 5
19					0.45	0.141 4
20					0.65	0.204 2
21					0.85	0.267 0
22					1.05	0.329 9
23					1.25	0.392 7
24				SIN2	0.05	0.02
25					0.25	0.10
26					0.45	0.18
27					0.65	0.26
28					0.85	0.34
29					1.05	0.42
30					1.25	0.50

The flow parameters for different cases used in the present work are summarized in Table II. Cases 1 and 2 are used to simulate the experiment in Krieg and Mohseni<sup>14</sup> to verify the numerical method used in the present work. The linear acceleration scheme is used, which accelerates from 0.05 to 0.147 m/s at  $a = 0.083 \text{ m/s}^2$  for the nozzle configuration (case 1), and from 0.021 to 0.082 m/s at  $a = 0.029 \text{ m/s}^2$  for the orifice configuration (case 2). Cases 3 to 30 are used to verify the accuracy for the OP model, where cases 3 to 16 employ the nozzle configuration and cases 17 to 30 employ the orifice configuration. The acceleration scheme used by cases 3 to 9 and 17 to 23 is SIN, and the acceleration scheme used by cases 10 to 16 and 24 to 30 is SIN2. For each combination of acceleration scheme and configuration, a total of seven cases with different acceleration stage stroke ratios ( $L_a/D = 0.05 : 0.2 : 1.25$ ) are carried out by modifying the acceleration time  $t_a$  in velocity function.

**FIG. 2.** Jet velocity and acceleration against time under different acceleration schemes for cases with  $L_a/D = 1.25$ . "SIN" indicates the first acceleration scheme, see Eq. (27); "SIN2" indicates the second acceleration scheme, see Eq. (28).

Similar to Zhu *et al.*<sup>37</sup> and Gao *et al.*,<sup>38</sup> ANSYS Fluent 19.2 has been used for all numerical simulations in the present work. Incompressible laminar flow assumption is applied due to the low Reynolds number. The Reynolds number is less than 2 700 when the jet inflow boundary diameter  $D$  and the maximum jet velocity  $U_{0max}$  are used as the characteristic length and velocity, respectively,

$$Re = \frac{U_{0max}D}{\gamma}, \quad (30)$$

where  $\gamma$  is the kinematic viscosity of liquid water. The computational domain is discretized using a non-uniform rectangular grid and encrypted at the shear and boundary layers. The total circulation of starting jet  $\Gamma_{total}$  at  $t^* = 0.4715$  ( $t = 0.1 \text{ s}$ ) would be compared in the grid independence and temporal convergence tests because the total jet circulation is of most interest in the present work.  $t^*$  is the formation time suggested by Gharib *et al.*,<sup>11</sup> i.e.,

$$t^* = \frac{\int_0^t U_0(t)dt}{D}. \quad (31)$$

The relevant parameters and results of the grid independence and time convergence tests are summarized in Table III. The total circulation of starting jet at  $t^* = 0.4715$  in the nozzle and orifice configurations for the three grids exhibits less than 1% difference between the two finest grids. Therefore, the grids with 59 826 and 58 866 nodes would be used for nozzle and orifice configurations. There is almost no difference between the two shortest time steps (the relative error is 0.000 45%), and the fixed time step of  $\Delta t = 0.1 \text{ ms}$  would be used for all subsequent numerical simulations.

The correctness of the numerical method has been verified by comparing with the experimental results by Krieg and Mohseni<sup>14</sup> for nozzle and orifice configurations with a linear acceleration scheme. The comparison of the total starting jet circulation produced by the nozzle (orifice) configuration in the experiment by Krieg and Mohseni<sup>14</sup> and simulation (denoted as CFD) in the present work is

**TABLE III.** Summary of the parameters and results for grid independence and temporal convergence tests. The relative error is calculated by taking the finest grid or the minimum time step as the accurate value.

	Configuration	Nodes	$\Delta t$ (ms)	$\Gamma(t^* = 0.4715)$ (cm <sup>2</sup> /s)	Relative error (%)
Grid independence	Nozzle (case 3)	29 256	0.10	11.420 30	3.895 34
		59 826	0.10	10.967 77	0.221 52
		95 634	0.10	10.992 12	...
	Orifice (case 17)	25 971	0.10	20.956 55	2.115 89
		58 866	0.10	20.575 95	0.261 33
		99 477	0.10	20.522 32	...
Temporal convergence	Nozzle (case 3)	59 826	0.20	10.967 61	0.001 92
		59 826	0.10	10.967 77	0.000 45
		59 826	0.05	10.967 82	...

shown in Fig. 3. Based on the assumption of axisymmetric flow, the total circulation of the non-impulsive starting jet can be directly obtained from the azimuthal vorticity distribution in the  $x-r$  plane,<sup>51</sup> as follows:

$$\Gamma_{total} = \int_A \omega_\theta r dx, \quad (32)$$

where  $A$  is the area outside the nozzle (orifice) configuration, and  $\omega_\theta$  is the azimuthal component of vorticity, i.e.,

$$\omega_\theta = \frac{\partial v}{\partial x} - \frac{\partial u}{\partial r}. \quad (33)$$

The good agreement between simulation and experimental results verifies the correctness of the numerical method used in the present work and ensures that the error with the numerical method is within 5%.

## IV. NUMERICAL RESULTS AND DISCUSSION

### A. Evolution of circulation growth in non-impulsive starting jet

Two methods have been mentioned above to calculate the total circulation of the non-impulsive starting jet. One is to integrate directly the azimuthal vorticity field obtained by numerical simulation based on the flow axisymmetric assumption, see Eq. (32).<sup>51</sup> The other is directly determined by the parameters at the jet inflow boundary obtained by numerical simulation, see Eq. (8). It is believed that the circulation growth of the starting jet depends on three factors, namely, the velocity and gauge pressure at the center of the jet inflow boundary, and the variation of radial velocity distribution in the jet inflow boundary. Therefore, the total circulation of the starting jet can be divided into three components based on Eq. (8), i.e.,

$$\Gamma_{total} = \Gamma_u + \Gamma_p + \Gamma_{dv/dt}, \quad (34)$$

where  $\Gamma_u$  and  $\Gamma_p$  can be calculated by Eqs. (14) and (15), respectively, and

$$\Gamma_{dv/dt} = - \int_0^{R_\infty} v(t, r)|_{x=0} dr. \quad (35)$$

Therefore, the three components on the right-hand side of Eq. (34) can be calculated from  $u_d$ ,  $P_d$ , and  $v(t, r)|_{x=0}$  obtained by numerical simulation. Krueger<sup>35</sup> obtained an over-pressure correction model that can calculate the total circulation of the impulsive starting jet by modeling  $\Gamma_u$  and  $\Gamma_p$ , respectively, but omitting  $\Gamma_{dv/dt}$ . The OP model also uses the assumption that the variation of radial velocity

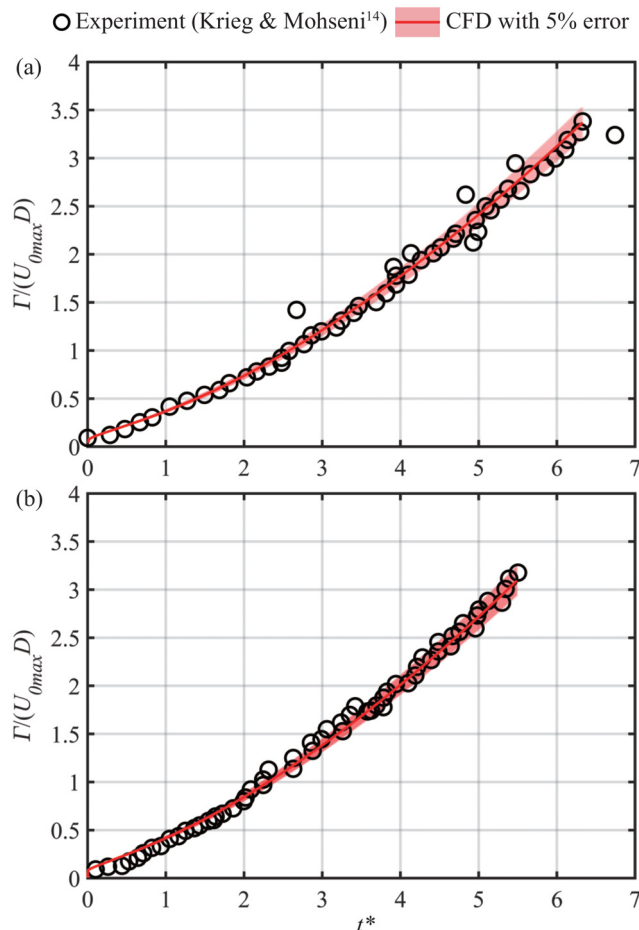


**FIG. 3.** Comparison of the circulation between CFD results in the present work (with 5% error) and experimental results of Krieg and Mohseni:<sup>14</sup> (a) is the nozzle configuration (case 1) and (b) is the orifice configuration (case 2).



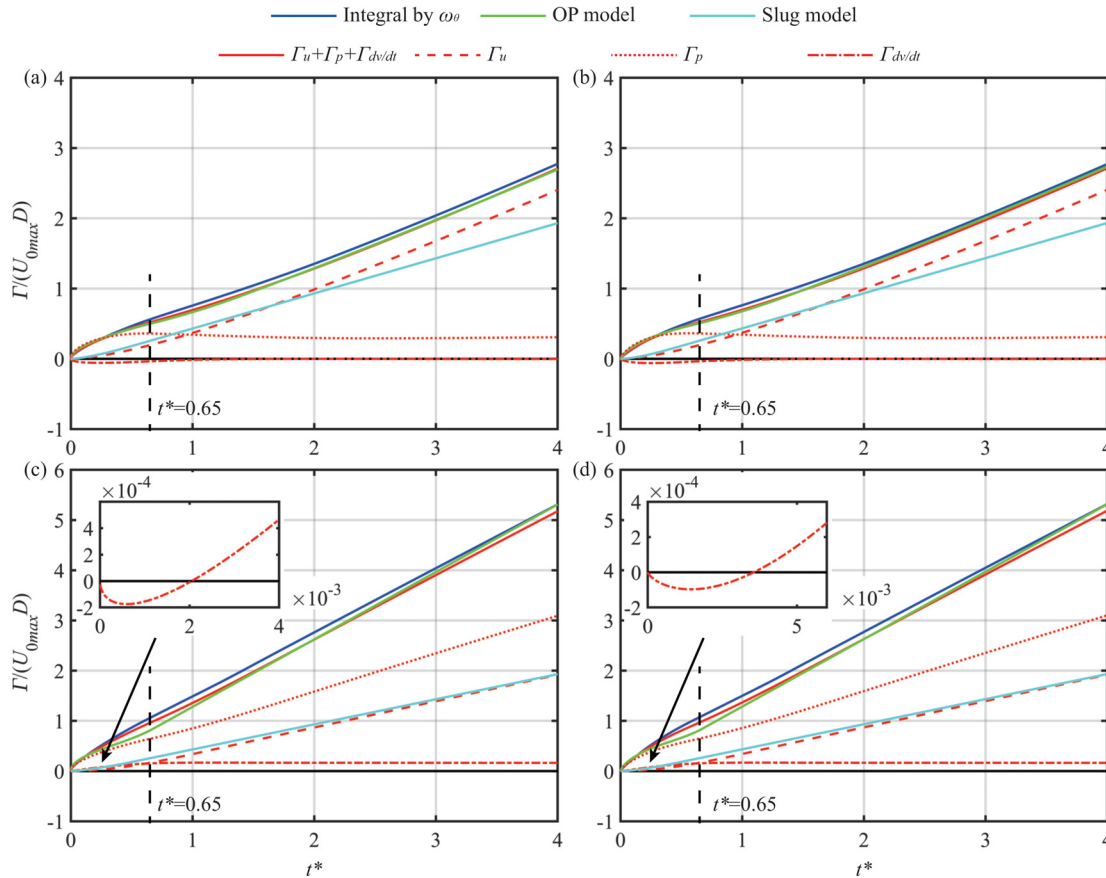


**FIG. 4.** The circulation growth process of non-impulsive starting jet ( $L_a/D = 0.65$ ) in different configurations (nozzle and orifice) and acceleration schemes (SIN and SIN2): (a) case 6 (nozzle with SIN scheme); (b) case 13 (nozzle with SIN2 scheme); (c) case 20 (orifice with SIN scheme); and (d) case 27 (orifice with SIN2 scheme). The blue and red lines are obtained from the numerical simulation results; the green and cyan lines are obtained based on the jet velocity  $U_0(t)$  by the OP model and the slug model, respectively.

distribution in the jet inflow boundary has a limited effect on the circulation growth of the non-impulsive starting jet.

Figure 4 presents the total circulation growth process of the non-impulsive starting jet formed by different acceleration schemes (SIN and SIN2) and configurations (nozzle and orifice) at  $L_a/D = 0.65$ , which are calculated by Eqs. (8) and (32) from numerical simulation results or predicted by the OP model proposed in the present work and the classical slug model from the known  $U_0(t)$ . The shadow of error within numerical results (5%) is excluded from Fig. 4 to avoid excessive clutter. The three components on the right-hand side of Eq. (34) calculated from numerical simulation results are also given separately. It is shown that the total circulation of the non-impulsive starting jet obtained from Eq. (8) derived by Krueger<sup>35</sup> (red solid line) is almost identical to the integral of the azimuthal component of the vorticity (blue solid line). Comparing the first component  $\Gamma_u$  (red dashed line) to the slug model (cyan solid line), which is equivalent to comparing the velocity at the center of the jet inflow boundary  $u_{cl}(t)$  and the jet velocity  $U_0(t)$ , it can be found that it is more consistent in the orifice configuration than that in the nozzle configuration by comparing Figs. 4(a) and 4(c) and Figs. 4(b) and 4(d). This is due to the fact

that the continuous growth of the boundary layer in the nozzle configuration causes the velocity of the jet core to accelerate under the constraints of the incompressible continuity equation.<sup>16,30,31</sup> However, the flow contraction at the jet inflow boundary due to the orifice configuration tends to interrupt the boundary layer growth.<sup>16,17,40</sup> The phenomenon that  $u_{cl}(t)$  is smaller than  $U_0(t)$  in the early stage ( $t^* < 1.8$  for nozzle and  $t^* < 3$  for orifice) is also consistent with previous research results.<sup>19,35,40,52</sup> The nozzle and orifice configurations produce different trends in the second component  $\Gamma_p$  (red dotted line), compare Figs. 4(a) and 4(c) or Figs. 4(b) and 4(d). During the acceleration stage ( $t^* < 0.65$ ),  $\Gamma_p$  grows with almost the same trend in both configurations. After that,  $\Gamma_p$  in the nozzle configuration first decreases slightly and then remains unchanged after a period of time, while  $\Gamma_p$  in the orifice configuration continues to increase at a certain growth rate. The trend for the third component  $\Gamma_{dv/dt}$  (red dash-dotted line) in the non-impulsive starting jet produced by the two configurations is the same, but the final results are different. The value of  $\Gamma_{dv/dt}$  first decreases to negative and then increases to a constant value, which is close to 0 for the nozzle configuration [Figs. 4(a) and 4(b)] and positive for the orifice configuration [Figs. 4(c) and 4(d)].

In addition, the proportion of  $\Gamma_{dv/dt}$  to  $\Gamma_{total}$  in the whole process is very small, which is far less than 10% for both configurations, so it is reasonable to ignore this component when constructing the OP model.

Finally, we turn our attention to the results calculated by the OP model (green solid line in Fig. 4) proposed in the present work. The contraction coefficient  $C_c$  used by the OP model in the orifice configuration was 0.61 based on  $D/D_t = 0.5$  from Vennard<sup>53</sup> and Krueger.<sup>35</sup> Comparing with the classic slug model (cyan solid line), the OP model proposed in the present work can better predict the circulation growth of the non-impulsive starting jet, which is almost coincident with the  $\Gamma_{total}$  obtained from the numerical simulation results (the red and blue solid lines in Fig. 4) in the whole process. At  $t^* = 4$ , the error between the total circulation predicted by the slug model and that obtained by the numerical simulation is about 30% for the nozzle configuration and 65% for the orifice configuration, which is consistent with the conclusions obtained by Krueger<sup>35,40</sup> and Krieg and Mohseni.<sup>13</sup> However, the errors with the results predicted by the OP model are less than 5% for the non-impulsive starting jets generated by the two configurations. This also proves that the OP model can hold beyond the assumption of small  $L_a/D$  ( $L_a/D \ll 1$ ) without increasing huge errors.

The variation of the second component  $\Gamma_p$  is only related to the gauge pressure at the center of the jet inflow boundary  $P_d(t)$ , see Eq. (15).  $\Gamma_p$  would increase when  $P_d(t)$  is positive and vice versa.

Figure 5 shows the pressure field near the jet inflow boundary for nozzle (case 6) and orifice (case 20) configurations at  $t^* = 0.18$ ,  $t^* = 0.88$ , and  $t^* = 2.25$ . Comparing with the red dotted line in Fig. 4, the above three instants correspond to the three stages with different growth rates of  $\Gamma_p$ . At  $t^* = 0.18$ , the pressure in the jet inflow boundary is mainly positive due to the acceleration of the jet, and the gauge pressure at its edge is negative due to the formation of the leading vortex ring,<sup>38</sup> regardless of the nozzle or orifice configuration, see Figs. 5(a) and 5(d). This is the reason why  $\Gamma_p$  grows during the jet acceleration stage ( $t^* < 0.65$ ). Similar to the results from Gao *et al.*,<sup>38</sup> the negative pressure region induced by the leading vortex ring continuously expands with its development, resulting in a completely negative pressure region in the jet inflow boundary of the nozzle configuration, as shown in Fig. 5(b). After that, the pressure in the jet inflow boundary is close to zero after the leading vortex ring convects away from there, see Fig. 5(c). At the same time, a weaker positive pressure area appears in the central region of the nozzle.<sup>54</sup> The reemergence of the positive pressure region can be attributed to the continuous acceleration of the jet core region due to the growth of the boundary layer on the nozzle wall, while the effect of the leading vortex ring has disappeared. However, for the orifice configuration, even after the jet acceleration stage is finished, the gauge pressure at the jet inflow boundary is still positive due to the structure-induced streamline curvature, see Figs. 5(e) and 5(f).<sup>13,35</sup> This positive pressure will also accelerate the fluid between the jet inflow boundary and the *vena contracta*

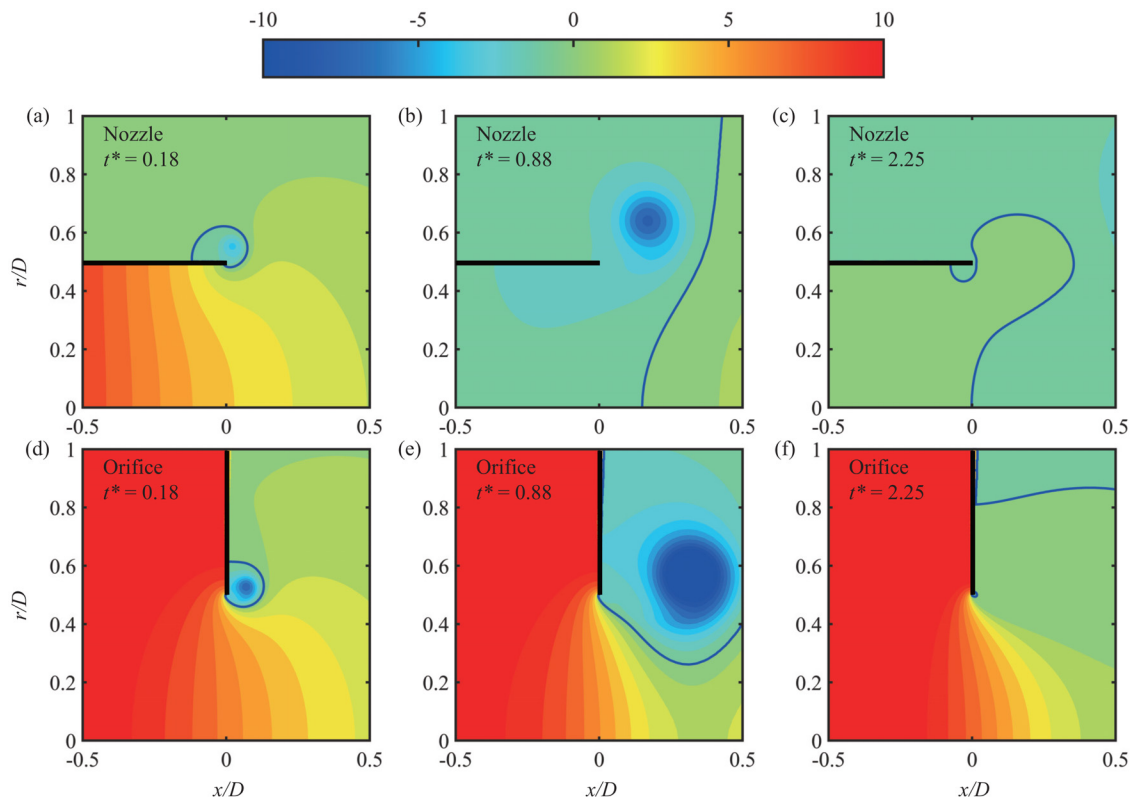


**FIG. 5.** The evolution of the pressure field near the jet inflow boundary for nozzle configuration [case 6, (a)–(c)] and orifice configuration [case 20, (d)–(f)]. The solid blue lines represent contour lines with pressure equal to 0, which is used to distinguish positive and negative pressure regions.

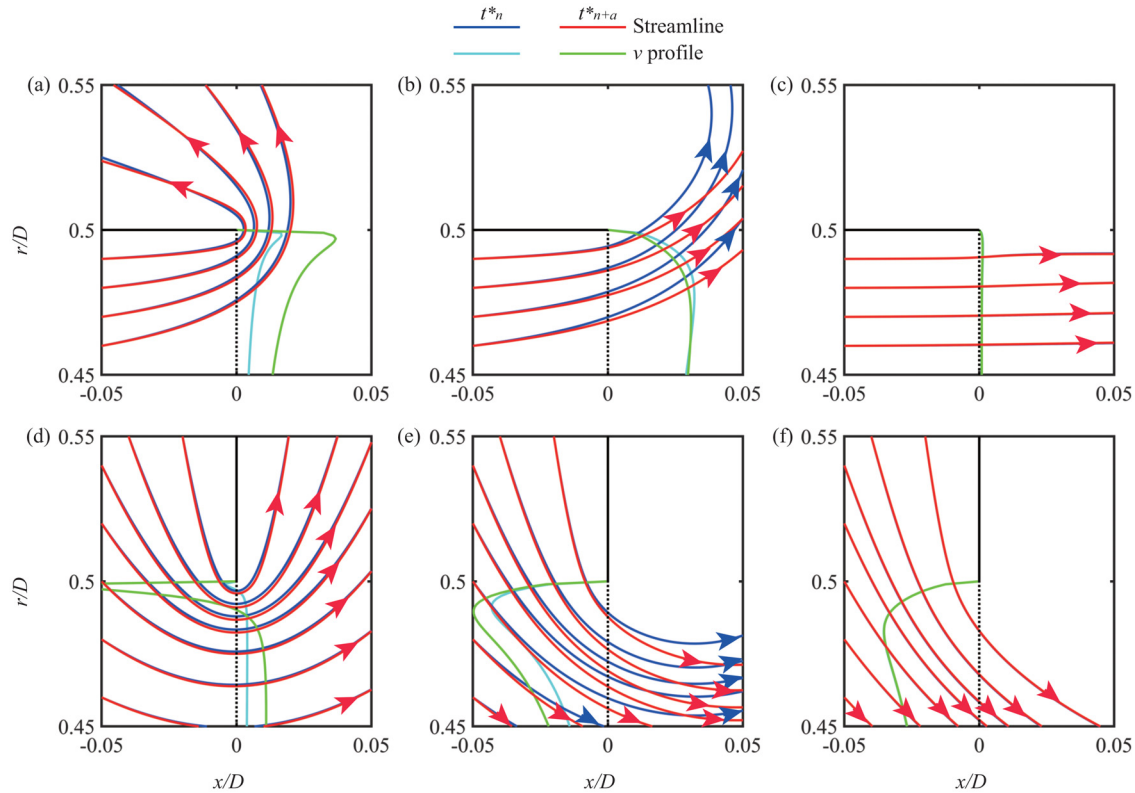


**FIG. 6.** The evolution of the streamlines and radial velocity profiles near the jet inflow boundary for nozzle configuration [case 6, (a)–(c)] and orifice configuration [case 20, (d)–(f)]: (a) and (d)  $t_n^* = 0.00002$ ,  $t_{n+a}^* = 0.00017$ ; (b) and (e)  $t_n^* = 0.11924$ ,  $t_{n+a}^* = 0.18302$ ; (c) and (f)  $t_n^* = 2.62935$ ,  $t_{n+a}^* = 3.12935$ . The black dotted line represents the jet inflow boundary and the coordinate line for  $v = 0$  (the right side represents  $v$  radially outward).

via Bernoulli's equation. However, the negative pressure area induced by the existence of the leading vortex ring reduces the gauge pressure at the center of the jet inflow boundary  $P_{cl}(t)$  at  $t^* = 0.88$ . This is why the orifice configuration shows two stages in different growth rates of  $\Gamma_p$ , namely,  $0.65 < t^* < 1$  with a gradually increasing rate and constant  $t^* > 1$  after the completion of the jet acceleration stage.

The variation of the third component on the right-hand side of Eq. (34)  $\Gamma_{dvd t}$  is related to the radial velocity profile in the jet inflow boundary [see Eq. (35)], which appears to be related to the curvature of the streamlines there.<sup>13</sup> Therefore, it would be analyzed through the evolution process of the streamlines and radial velocity profiles near the jet inflow boundary shown in Fig. 6. Since the magnitude and sign of  $d\Gamma_{dvd t}/dt$  are related to the time derivative [see Eq. (36)], two adjacent instants are given in each subgraph of Fig. 6 for the sake of comparison,

$$\frac{d\Gamma_{dvd t}}{dt} = -\frac{\partial}{\partial t} \int_0^{R_\infty} v(t, r)|_{x=0} dr. \quad (36)$$

At the onset of the starting jet, the jets created by the nozzle and orifice configurations expand radially outward at the jet inflow boundary, with increasing radial velocity as the flow continues, see Figs. 6(a) and 6(d). This is the reason why  $\Gamma_{dvd t}$  would decrease from 0 to negative first. However, at this time, the streamlines at the edge of the orifice

configuration are bent toward the centerline due to structural constraints, and the radial velocity there is negative (radially inward).<sup>16</sup> This phenomenon develops rapidly as the flow continues, see the time  $t_{n+a}^* = 0.00017$  in Fig. 6(d) and  $t_n^* = 0.11924$  in Fig. 6(e). This would cause the minimum value of  $\Gamma_{dvd t}$  in the orifice configuration to be larger than that in the nozzle configuration, and  $\Gamma_{dvd t}$  becomes positive more quickly. Finally, the streamlines at the two adjacent instants coincide with each other, the radial velocity is completely less than 0 (radially inward), and the radial velocity profiles also coincide with each other in Fig. 6(f). This bending of streamlines in the orifice configuration is known as *vena contracta*.<sup>34,35</sup> In contrast, the starting jet formed by the nozzle configuration does not experience this process, and the radial velocity gradually decreases after a period of time, finally becoming 0, as shown in Figs. 6(b) and 6(c). The difference in the radial velocity profiles formed at the jet inflow boundary between the two configurations determines that  $\Gamma_{dvd t}$  is 0 for the nozzle configuration, while  $\Gamma_{dvd t}$  becomes positive in the orifice configuration.

## B. Verification of the OP model

To assess the accuracy of the prediction results from the OP model proposed in the present work, the results from numerical simulation would be used to be the reference to define relative error calculation methods, as follows:

$$e_r(t = T) = \frac{|\Gamma_{model}(t = T) - \Gamma_{CFD}(t = T)|}{\Gamma_{CFD}(t = T)}, \quad (37)$$

where  $\Gamma_{model}(t = T)$  is the total circulation of the starting jet at a certain instant predicted by the model based on the starting jet velocity  $U_0(t)$ , and  $\Gamma_{CFD}(t = T)$  is obtained by integrating the vorticity field obtained from the numerical simulation results. To verify the ability of OP model to predict the transient process of circulation growth in the non-impulsive starting jet acceleration stage, the time-averaged relative error of the model will be used, i.e.,

$$\bar{e}_r = \frac{\sum_{T=1 \times dt}^{n \times dt} \frac{|\Gamma_{model}(t = T) - \Gamma_{CFD}(t = T)|}{\Gamma_{CFD}(t = T)}}{n}, \quad (38)$$

where  $dt$  is the time interval between instants selected for the calculation, and  $n$  is the number of instants selected. To fully include the acceleration stage of all cases, as well as uniformity, the following calculations about the time-averaged relative error  $\bar{e}_r$  take  $dt = 0.5$  ms and  $n = 1000$  (the maximum duration of the acceleration stage is 0.5 s for cases 16 and 30 with  $L_a/D = 1.25$ , see Table II).

The time-averaged relative error  $\bar{e}_r$  and the relative error at the end of the acceleration stage  $e_r(t^* = L_a/D)$  within the results obtained by the OP model are shown in Fig. 7 for cases 3–30. For comparison, the error within the results obtained by the classical slug model calculated according to Eq. (1) is also added. As shown, the OP model greatly improves the accuracy of the prediction. The time-averaged relative error  $\bar{e}_r$  range of the OP model is about 11% to 26% for cases 3–30, which is much smaller than that of the slug model from 44% to 88% [Fig. 7(a)]. In addition, the difference between the prediction errors  $e_r$  of the OP model for the nozzle and orifice configurations with the same jet velocity  $U_0(t)$  is also not large, about 4% to 10%, while the difference in the error of the slug model between the two configurations is about 15% to 35%. When  $L_a/D$  changes from 0.05 to 1.25,  $\bar{e}_r$  of the OP model decreases continuously for the acceleration scheme SIN, but increases continuously for the acceleration scheme SIN2. However, the variation of  $\bar{e}_r$  caused by different  $L_a/D$  is less than 5%. This demonstrates the same applicability of the OP model to the non-impulsive starting jets with different  $L_a/D$ .

Next, we will focus on the relative error at the end of the acceleration stage  $e_r(t^* = L_a/D)$ , as shown in Fig. 7(b). For both SIN and SIN2 acceleration schemes, the  $e_r(t^* = L_a/D)$  is almost the same, whether it is the OP model or the slug model. For the scope  $L_a/D$  in this study from 0.05 to 1.25,  $e_r(t^* = L_a/D)$  of the OP model is 4% to 28%, which is smaller than that of the slug model from 39% to 96%. The acceleration of the jet decreases, and the over-pressure effect weakens due to the increase in  $L_a/D$ .<sup>11</sup> The  $e_r(t^* = L_a/D)$  of the slug model gradually decreases to about 39% for the nozzle configuration and to about 69% for the orifice configuration. Finally, it would be considered whether the prediction errors of the OP model accumulate for long-duration starting jet. The relative errors  $e_r(t^* = 4)$  for cases 3–30 are shown in Fig. 7(c). Comparing Figs. 7(b) and 7(c), it can be found that the relative error of the OP model does not increase from  $t^* = L_a/D < 4$  to  $t^* = 4$ , but decreases slightly. Therefore, it can be considered that the relative error of the OP model does not continue to grow if longer durations are considered. In addition, the reason why  $e_r(t^* = 4)$  is smaller than  $e_r(t^* = L_a/D)$  can be considered as the higher accuracy

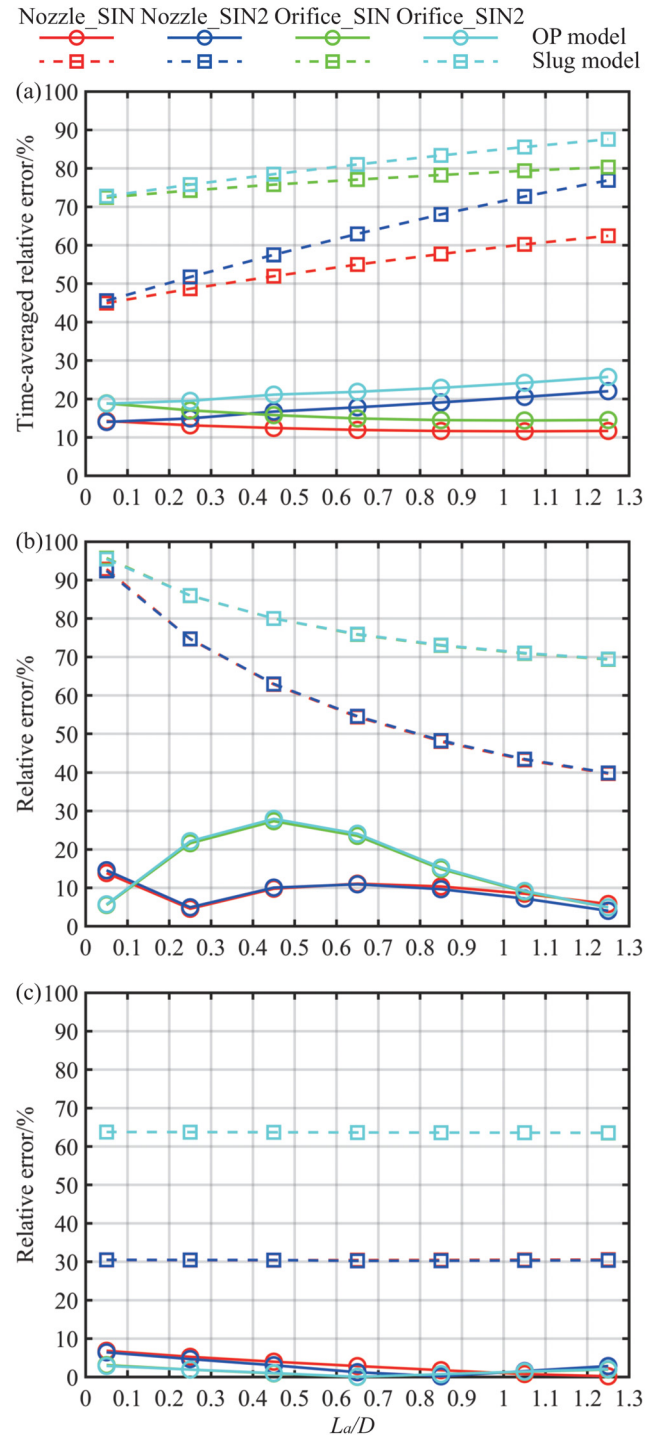


**FIG. 7.** (a) Time-averaged relative error  $\bar{e}_r$ , (b) the relative error at the end of the acceleration stage  $e_r(t^* = L_a/D)$ , and (c) the relative error at  $t^* = 4$   $e_r(t^* = 4)$  in different acceleration stage stroke ratio  $L_a/D$ . NOZZLE\_SIN is nozzle with SIN scheme (cases 3–9); NOZZLE\_SIN2 is nozzle with SIN2 scheme (cases 10–16); ORIFICE\_SIN is orifice with SIN scheme (cases 17–23); and ORIFICE\_SIN2 is orifice with SIN2 scheme (cases 24–30).



of the OP model in predicting the circulation growth of the starting jet with a constant jet velocity after  $t^* = L_a/D$ .

### C. Refinement of the OP model

#### 1. Nozzle configuration

In the process of constructing the OP model in Sec. II, only the first two items on the right-hand side of Eq. (8) are considered, i.e.,  $\Gamma_u$  and  $\Gamma_p$ , while  $\Gamma_{dv/dt}$  is ignored [see Eq. (19)]. Therefore, the rationality of ignoring  $\Gamma_{dv/dt}$  and the prediction accuracy of the OP model for  $\Gamma_u$  and  $\Gamma_p$  would be discussed below.

The key to model  $\Gamma_u$  is to accurately obtain the centerline velocity  $u_{cl}(t)$ , see Eq. (21).  $u_{cl}(t)$  can be obtained using Eq. (22) in combination with Eqs. (2) and (24) in the nozzle configuration. The  $u_{cl}(t)$  predicted by the OP model with the two acceleration schemes (SIN in case 6 and SIN2 in case 13) and that obtained from the numerical simulation results are compared in Fig. 8(a). It can be seen that the OP model can accurately predict  $u_{cl}(t)$  in the non-impulsive starting jet. The most pronounced prediction error appears around  $t^* = 1.42$ , which can be attributed to the error introduced by the used transition function  $\sigma_n(t)$  [Eq. (24)]. The time-averaged relative errors  $\bar{e}_r$  within the results  $\Gamma_u$  predicted by the OP model for cases 3–16 are shown in Fig. 8(b), and the  $\bar{e}_r$  within  $\Gamma_{total}$  is also given for comparison. The OP model predicts  $\Gamma_u$  with  $\bar{e}_r$  ranging from 7.5% to 13%. When  $L_a/D = 0.05$ , which is the smallest stroke ratio in the acceleration stage,  $\bar{e}_r$  within  $\Gamma_u$  is almost the same as  $\Gamma_{total}$ , but it becomes smaller than that within  $\Gamma_{total}$  with the increase in  $L_a/D$ .

Based on Eq. (15), it can be obtained that the prediction of  $\Gamma_p$  can be characterized as the prediction of  $P_{cl}$ . The over-pressure correction term for the non-impulsive starting jets in the OP model is the second term on the right-hand side of Eq. (18), which can be equivalent to Eq. (15) to obtain

$$\int_0^t \frac{a(t)dtD}{\pi} = \int_0^t \frac{P_{cl}(t)}{\rho} dt. \quad (39)$$

By removing the integral sign, we can obtain

$$P_{cl} = \rho \frac{a(t)D}{\pi}. \quad (40)$$

The acceleration used in Eqs. (39) and (40) is obtained by differentiating the jet velocity  $U_0(t)$  with respect to time  $t$ . However, the translating disk analytical solution used by Krueger<sup>35</sup> in deriving the over-pressure correction term is based on the irrotationality assumption of the jet core.<sup>50,55</sup> Therefore, the acceleration obtained by differentiating the core velocity  $U_c(t)$  with respect to time  $t$ , which has taken into account the correction of the boundary layer, may be better to approximate  $P_d$ . The  $P_d(t)$  obtained from the numerical simulation results and calculated using Eq. (40), where the acceleration is obtained according to  $U_0(t)$  and  $U_c(t)$ , respectively, are shown in Fig. 9(a) for cases 6 and 13. The over-pressure correction term derived for the impulsive starting jet can be extended to the non-impulsive starting jet, and the predicted  $P_d(t)$  is very close to the numerical simulation results. Using the core velocity  $U_c(t)$  instead of the jet velocity  $U_0(t)$  to obtain the acceleration has better accuracy, whether in the jet acceleration stage or the prediction of the positive pressure caused by the boundary layer growth in the later stage.

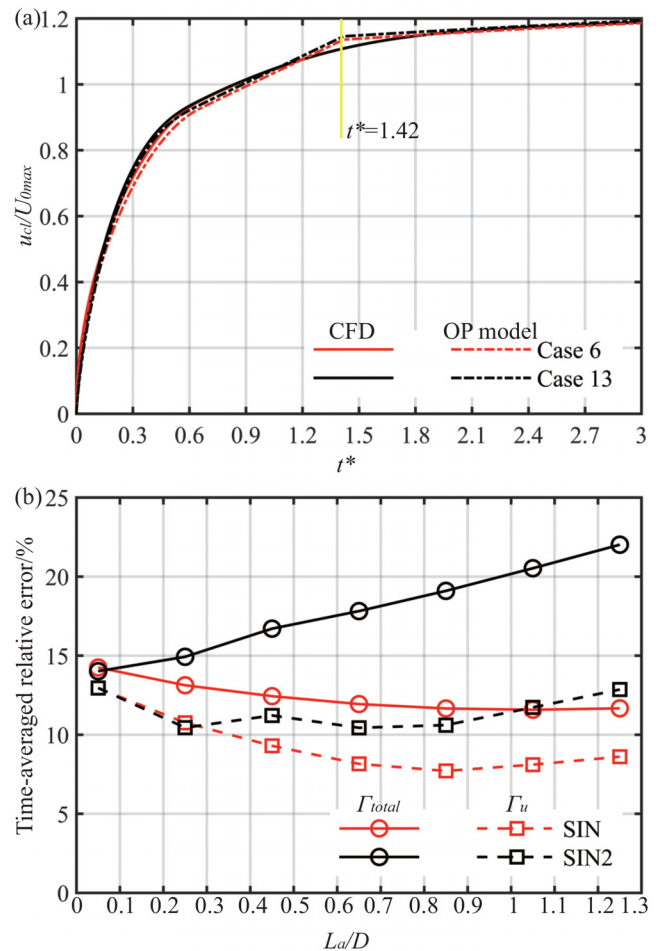


**FIG. 8.** (a) Comparison of the centerline velocity  $u_{cl}(t)$  predicted by the OP model and that from the numerical simulation results under the two acceleration schemes (SIN in case 6, SIN2 in case 13) and (b) comparison of the time-averaged relative errors within  $\Gamma_{total}$  (solid line) and  $\Gamma_u$  (dash line) obtained by the OP model for cases 3–9 with SIN (red line) and cases 10–16 with SIN2 (black line).

The error of the OP model in predicting  $\Gamma_p$  and the effect of ignoring  $\Gamma_{dv/dt}$  would be discussed. The  $\Gamma_p$  and  $\Gamma_p + \Gamma_{dv/dt}$  obtained from CFD (with 5% error) by Eqs. (15) and (35) and  $\Gamma_p$  calculated by the OP model [using  $U_0(t)$ ] for case 6 are shown in Fig. 9(b). It can be seen that the  $\Gamma_p$  calculated by the OP model is underestimated when  $t^* < 1.5$  and overestimated when  $t^* > 1.5$  compared with the  $\Gamma_p$  obtained from the numerical simulation results. On the contrary, comparing with the  $\Gamma_p$  obtained from the numerical simulation results, the  $\Gamma_p + \Gamma_{dv/dt}$  obtained from the numerical simulation results seems to be closer to the  $\Gamma_p$  calculated by the OP model. The time-averaged relative errors  $\bar{e}_r$  of the  $\Gamma_p$  calculated by the OP model with respect to  $\Gamma_p$  and  $\Gamma_p + \Gamma_{dv/dt}$  obtained from the numerical simulation results are shown in Fig. 9(c) for cases 3–16. The  $\bar{e}_r$  of the OP model in predicting  $\Gamma_p$  ranges from 7% to 12%, which is comparable to the  $\bar{e}_r$  with  $\Gamma_u$ . The  $\bar{e}_r$  of  $\Gamma_p$  obtained by the OP model relative to  $\Gamma_p + \Gamma_{dv/dt}$  obtained from the numerical simulation results ranges from 5% to 15.5%. In some cases, such as at  $L_a/D = 0.05$ , the difference between



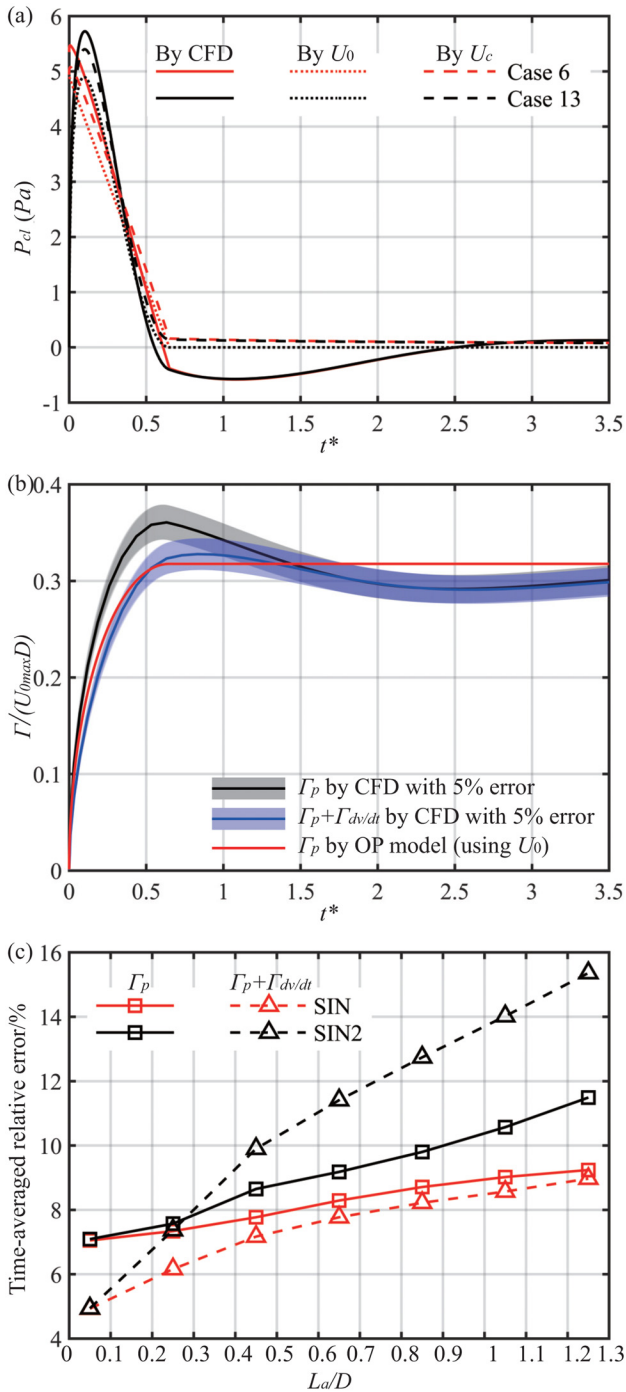


**FIG. 9.** (a) Comparison of  $P_{cl}$  predicted by the OP model [using the jet velocity  $U_0(t)$  and core velocity  $U_c(t)$  to obtain the acceleration  $a(t)$ , respectively] and that from the CFD results under the two acceleration schemes (SIN in case 6 and SIN2 in case 13); (b) comparison of  $\Gamma_p$  calculated by the OP model with  $\Gamma_p$  and  $\Gamma_p + \Gamma_{dv/dt}$  obtained from CFD (with 5% error) for case 6; (c)  $\bar{e}_r$  of  $\Gamma_p$  obtained by the OP model relative to  $\Gamma_p$  (solid line) and  $\Gamma_p + \Gamma_{dv/dt}$  (dash line) obtained from the numerical simulation results, respectively, for cases 3–9 with SIN (red line) and cases 10–16 with SIN2 (black line).

$\Gamma_p$  obtained by the OP model and  $\Gamma_p + \Gamma_{dv/dt}$  obtained from the numerical simulation results is smaller than the difference between  $\Gamma_p$  obtained by the OP model and  $\Gamma_p$  obtained from the numerical simulation results. This is because the OP model underestimates  $P_{cl}(t)$  and  $\Gamma_p$  during the acceleration stage [see Figs. 9(a) and 9(b)], but the  $\Gamma_{dv/dt}$  is negative at this time (Fig. 4). This can compensate for the error caused by ignoring  $\Gamma_{dv/dt}$  during model derivation. In general, the error caused by ignoring  $\Gamma_{dv/dt}$  does not exceed 5% (comparable to the error with the numerical simulation method), so it is reasonable to ignore this item in the process of constructing this model.

## 2. Orifice configuration

For the orifice configuration, the gauge pressure at the jet inflow boundary remains positive as a result of the curvature of the resulting streamlines even though the jet acceleration stage has already stopped. When constructing the OP model for the orifice configuration, the  $u_{cl}$  at the *vena contracta* was used instead of the  $u_{cl}$  at the jet inflow boundary, so that the phenomenon of  $P_{cl} > 0$  caused by the flow contraction can be compensated. This makes  $\Gamma_u$  and  $\Gamma_p$  predicted by the OP model not correspondingly equal to  $\Gamma_u$  and  $\Gamma_p$  calculated by Eqs. (14) and (15) from the numerical simulation results. However, the sum of  $\Gamma_u$  and  $\Gamma_p$  predicted by the OP model and that calculated from numerical simulation results are comparable. According to Eq. (34),  $\Gamma_u + \Gamma_p$  is equal to  $\Gamma_{total} - \Gamma_{dv/dt}$ . To study the effect of ignoring  $\Gamma_{dv/dt}$  in the orifice configuration, the  $\Gamma_{total}$  and  $\Gamma_{total} - \Gamma_{dv/dt}$  obtained from the numerical results and the  $\Gamma_{total}$  calculated by the OP model are shown in Fig. 10(a) for case 20. It can be found that the OP model ignoring  $\Gamma_{dv/dt}$  would cause a relatively obvious error around  $t^* = 0.5$ . However, this error will gradually decrease or even disappear as the jet continues. The time-averaged relative errors  $\bar{e}_r$  between  $\Gamma_{total}$  calculated by OP model and  $\Gamma_{total}$  and  $\Gamma_{total} - \Gamma_{dv/dt}$  calculated from the numerical simulation results are shown in Fig. 10(b). It can be seen that  $\bar{e}_r$  between the  $\Gamma_{total}$  calculated by the OP model and the  $\Gamma_{total} - \Gamma_{dv/dt}$  obtained from the numerical simulation results is between 5% and 19%.  $\bar{e}_r$  between the  $\Gamma_{total}$  calculated by the OP model and the  $\Gamma_{total}$  obtained from the numerical simulation results is between 14% and 26%. Comparing each case (the same color and  $L\alpha/D$ ) in Fig. 10(b), it can be found that ignoring  $\Gamma_{dv/dt}$  would increase  $\bar{e}_r$  by less than 14%. This is more serious than that in the nozzle configuration, which can be attributed to that the nozzle configuration does not cause streamlines to bend and  $\Gamma_{dv/dt}$  is close to 0 after the acceleration stage. However,  $\Gamma_{dv/dt}$  experiences a short-term decrease and then rapidly increases to a relatively large positive value in the orifice configuration, see Figs. 4(c) and 4(d). This may be the reason why ignoring  $\Gamma_{dv/dt}$  in the orifice configuration would induce a larger error.

In constructing the OP model of the orifice configuration, the transition function [Eq. (26)] from Krueger<sup>35</sup> has been used to complete the model. After that, Krueger<sup>40</sup> had fitted a new transition function by studying the relationship between the axial displacement of the leading vortex ring and the dimensionless time  $t^*$  [equal to  $L(t)/D$ ] for the impulsive starting jet generated by the orifice configuration, as follows:

$$\sigma_n(t) = \begin{cases} 1.118(L(t)/D)^{0.25}, & L(t)/D < 0.64, \\ 1, & L(t)/D \geq 0.64. \end{cases} \quad (41)$$

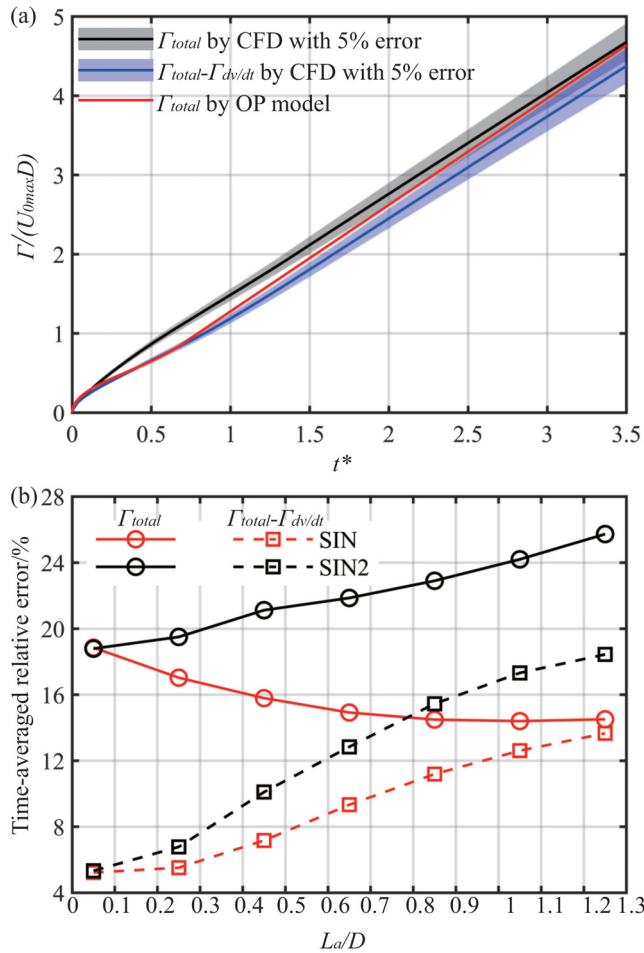


**FIG. 10.** (a) Comparison of  $\Gamma_{total}$  and  $\Gamma_{total} - \Gamma_{dv/dt}$  obtained from CFD (with 5% error) with  $\Gamma_{total}$  calculated by the OP model for case 20 and (b) the time-averaged relative errors of the prediction result from the OP model with respect to  $\Gamma_{total}$  (solid line) and  $\Gamma_{total} - \Gamma_{dv/dt}$  (dash line) from the numerical simulation results, respectively, for cases 17–23 with SIN (red line) and cases 24–30 with SIN2 (black line).

Consider the jet velocity varying with time to apply this equation to non-impulsive starting jet when calculating  $L(t)$ . Therefore, instead of using Eq. (26), Eq. (41) can be applied to the OP model established in the present work. The revised model is denoted as the ROP model. The growth process of the total circulation obtained from numerical simulation results and that calculated by the OP model (red solid line) and ROP model (red dash line) are shown in Fig. 11(a). It can be seen that modifying the transition function can make the growth process of the total circulation calculated by the model closer to the results obtained by the numerical simulation. The time-averaged relative errors  $\bar{e}_r$  within the prediction results for cases 17–30 by the OP model and the ROP model are compared in Fig. 11(b). Comparing the prediction error of the OP and ROP model for each case [the same color and  $L_a/D$  in Fig. 11(b)], it can be found that  $\bar{e}_r$  of the ROP model is more than 5% lower than that of the OP model.

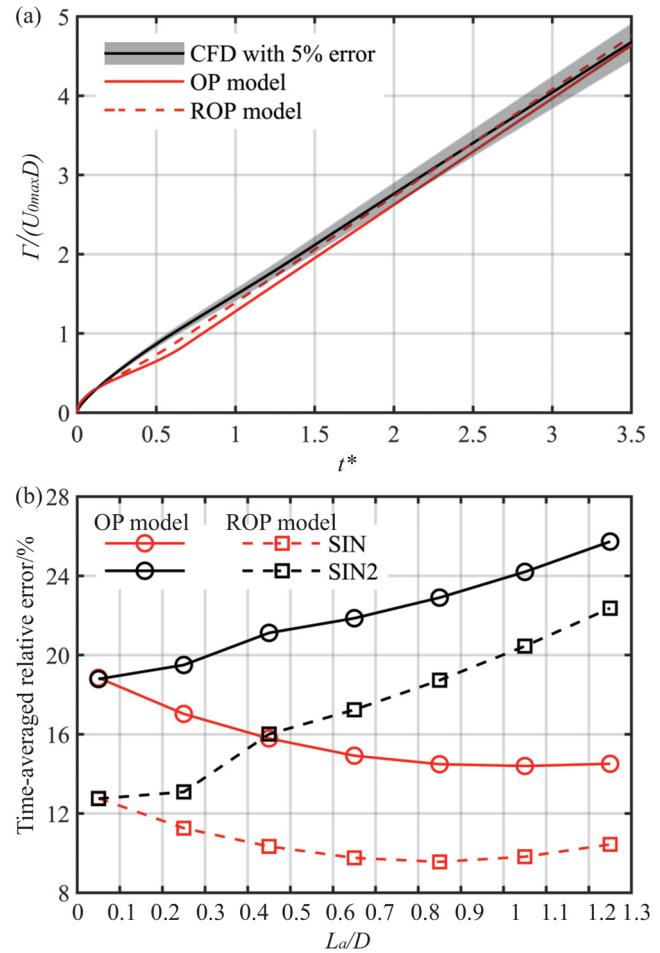


**FIG. 11.** (a) Comparison of the total circulation of starting jet obtained from CFD (with 5% error) with that calculated by the OP and ROP model for case 20 and (b) comparison of the time-averaged relative errors between the OP model (solid line) and the revised model (ROP) (dash line), for cases 17–23 with SIN (red line) and cases 24–30 with SIN2 (black line).

## V. CONCLUDING REMARKS

By extending the over-pressure correction model previously derived by Krueger<sup>35</sup> for impulsive starting jets, a model, denoted as OP model, that can predict the circulation growth process of the non-impulsive starting jets has been obtained, i.e.,

$$\Gamma_{total}(t) = \int_0^t \left[ \frac{1}{2} u_d^2(t) + \frac{a(t)D}{C_p} \right] dt. \quad (42)$$

Here,  $u_d$  can be calculated by Eq. (22) in the nozzle configuration and by Eq. (25) in the orifice configuration,  $a(t)$  is the jet acceleration obtained by differentiating the jet velocity  $U_0(t)$ , and  $D$  is the diameter of the jet inflow boundary. As for  $C_p$ , it is a constant  $\pi$  for the nozzle configuration and 2 for the orifice configuration. Two acceleration schemes combined with different acceleration stage stroke ratios

( $L_a/D = 0.05 : 0.2 : 1.25$ ) had been tested in the present work to verify the prediction accuracy of the model for the nozzle and orifice configurations. The results obtained by numerical simulation are used as a reference to calculate the relative error with the analytical model.

1. The dynamic process prediction error of this OP model, expressed as the time-averaged relative error over one thousand instants with a time interval of 0.5 ms (from  $t = 0.5$  ms to  $t = 0.5$  s), is 11% to 26%, which is smaller than the 44% to 88% of the classical slug model.
2. The error of the OP model in predicting the total circulation at the end of the acceleration stage of the non-impulsive starting jet, i.e., the relative error within  $\Gamma(t^* = L_a D)$ , is about 4% to 28%.
3. Krueger<sup>35</sup> proposed a constraint that the stroke ratio in the acceleration stage of the starting jet  $L_a/D$  should be much less than 1 for the over-pressure correction model. The prediction accuracy of the OP model would not decrease significantly with increasing  $L_a/D$  from 0.05 to 1.25, and the application range of our new model would not be limited by this constraint.

The total circulation of the starting jet is divided into three components ( $\Gamma_u$ ,  $\Gamma_p$ , and  $\Gamma_{dv/dt}$ ), and their evolution process and mechanism have also been examined. Then, the error sources of the OP model have been analyzed in combination with the three components, and attempts have been made to improve the model. In the process of constructing the OP model, based on the assumption that the influence of the component  $\Gamma_{dv/dt}$  caused by the change of radial velocity distribution is relatively small, it is, therefore, ignored and the OP model only considers  $\Gamma_u$  and  $\Gamma_p$ . The influence of ignoring  $\Gamma_{dv/dt}$  has also been discussed. For the nozzle configuration, neglecting  $\Gamma_{dv/dt}$  results in increasing the time-averaged relative error by less than 5%, and the time-averaged relative error of this model in the orifice configuration increases by 1% to 14%. For nozzle configuration, the key is to accurately predict the velocity at the centerline of the jet inflow boundary  $u_{cl}$  when predicting  $\Gamma_u$ , and the prediction of  $\Gamma_p$  can be deduced to the prediction of  $P_{cl}$ , so that we can obtain  $P_{cl}$  based only on the acceleration  $a(t)$  of the non-impulsive starting jet. The prediction of  $P_{cl}$  is more accurate using the acceleration  $a(t)$  derived from core velocity  $U_c(t)$  instead of jet velocity  $U_0(t)$ . For the orifice configuration, the model cannot predict  $\Gamma_u$  and  $\Gamma_p$  independently, but only the sum of them due to the existence of *vena contracta* phenomenon. In addition, the transition function used by the model for the orifice configuration was also modified, and the time-averaged relative error of the model was reduced by more than 5%.

## ACKNOWLEDGMENTS

This research has been carried out at the Beijing Institute of Technology, supported by the Funding Military Commission Equipment Development Department, Equipment Advance Research Field Fund (Grant Nos. 61407200113 and 61407200405) and State Administration of Science, Technology and Industry for National Defense, PRC (Grant No. JCKY2021602B025).

## AUTHOR DECLARATIONS

### Conflict of Interest

The authors have no conflicts to disclose.

## Author Contributions

**Jianwei Zhu:** Conceptualization (equal); Formal analysis (equal); Visualization (equal); Writing – original draft (equal). **G. Q. Zhang:** Data curation (equal); Funding acquisition (equal); Investigation (equal); Project administration (equal). **Lei Gao:** Methodology (equal); Resources (equal); Validation (equal). **Simon C. M. Yu:** Software (equal); Writing – review & editing (equal).

## DATA AVAILABILITY

The data that support the findings of this study are available from the corresponding author upon reasonable request.

## REFERENCES

- <sup>1</sup>E. J. Anderson and M. A. Grosenbaugh, "Jet flow in steadily swimming adult squid," *J. Exp. Biol.* **208**, 1125–1146 (2005).
- <sup>2</sup>H. Jiang and M. A. Grosenbaugh, "Numerical simulation of vortex ring formation in the presence of background flow with implications for squid propulsion," *Theor. Comput. Fluid Dyn.* **20**, 103–123 (2006).
- <sup>3</sup>I. K. Bartol, P. S. Krueger, W. J. Stewart, and J. T. Thompson, "Hydrodynamics of pulsed jetting in juvenile and adult brief squid *Lolliguncula brevis*: Evidence of multiple jet 'modes' and their implications for propulsive efficiency," *J. Exp. Biol.* **212**, 1889–1903 (2009).
- <sup>4</sup>J. O. Dabiri, "Optimal vortex formation as a unifying principle in biological propulsion," *Annu. Rev. Fluid Mech.* **41**, 17–33 (2009).
- <sup>5</sup>X. Bi and Q. Zhu, "Fluid-structure investigation of a squid-inspired swimmer," *Phys. Fluids* **31**, 101901 (2019).
- <sup>6</sup>X. Bi and Q. Zhu, "Pulsed-jet propulsion via shape deformation of an axisymmetric swimmer," *Phys. Fluids* **32**, 081902 (2020).
- <sup>7</sup>Y. Luo, Q. Xiao, Q. Zhu, and G. Pan, "Jet propulsion of a squid-inspired swimmer in the presence of background flow," *Phys. Fluids* **33**, 031909 (2021).
- <sup>8</sup>D. Greenblatt and I. J. Wygnanski, "The control of flow separation by periodic excitation," *Prog. Aerosp. Sci.* **36**, 487–545 (2000).
- <sup>9</sup>B. Steinfurth and J. Weiss, "Vortex rings produced by non-parallel planar starting jets," *J. Fluid Mech.* **903**, A16 (2020).
- <sup>10</sup>J. Töger, M. Kanski, M. Carlsson, S. J. Kovács, G. Söderlind, H. Arheden, and E. Heiberg, "Vortex ring formation in the left ventricle of the heart: Analysis by 4D flow MRI and Lagrangian coherent structures," *Ann. Biomed. Eng.* **40**, 2652–2662 (2012).
- <sup>11</sup>M. Gharib, E. Rambod, and K. Shariff, "A universal time scale for vortex ring formation," *J. Fluid Mech.* **360**, 121–140 (1998).
- <sup>12</sup>L. Gao and S. C. M. Yu, "Development of the trailing shear layer in a starting jet during pinch-off," *J. Fluid Mech.* **700**, 382–405 (2012).
- <sup>13</sup>M. Krieg and K. Mohseni, "Modelling circulation, impulse and kinetic energy of starting jets with non-zero radial velocity," *J. Fluid Mech.* **719**, 488–526 (2013).
- <sup>14</sup>M. Krieg and K. Mohseni, "A new kinematic criterion for vortex ring pinch-off," *Phys. Fluids* **33**, 037120 (2021).
- <sup>15</sup>R. Limbourg and J. Nedić, "An extended model for orifice starting jets," *Phys. Fluids* **33**, 067109 (2021).
- <sup>16</sup>R. Limbourg and J. Nedić, "An extension to the universal time scale for vortex ring formation," *J. Fluid Mech.* **915**, A46 (2021).
- <sup>17</sup>R. Limbourg and J. Nedić, "Formation of an orifice-generated vortex ring," *J. Fluid Mech.* **913**, A29 (2021).
- <sup>18</sup>P. G. Saffman, "On the formation of vortex rings," *Stud. Appl. Math.* **54**, 261–268 (1975).
- <sup>19</sup>N. Didden, "On the formation of vortex rings: Rolling-up and production of circulation," *Z. Angew. Math. Phys.* **30**, 101–116 (1979).
- <sup>20</sup>M. Nitsche and R. Krasny, "A numerical study of vortex ring formation at the edge of a circular tube," *J. Fluid Mech.* **276**, 139–161 (1994).
- <sup>21</sup>K. Mohseni and M. Gharib, "A model for universal time scale of vortex ring formation," *Phys. Fluids* **10**, 2436–2438 (1998).
- <sup>22</sup>M. Shusser, M. Gharib, and K. Mohseni, "A new model for inviscid vortex ring formation," in 30th Fluid Dynamics Conference, 1999.

- <sup>23</sup>L. Gao and S. C. M. Yu, "A model for the pinch-off process of the leading vortex ring in a starting jet," *J. Fluid Mech.* **656**, 205–222 (2010).
- <sup>24</sup>R. Limbourg and J. Nedić, "On the asymptotic matching procedure predicting the formation number," *Phys. Fluids* **33**, 117103 (2021).
- <sup>25</sup>T. B. Benjamin, "The alliance of practical and analytical insights into the non-linear problems of fluid mechanics," in *Applications of Methods of Functional Analysis to Problems in Mechanics* (Springer, 1976), pp. 8–29.
- <sup>26</sup>L. E. Fraenkel, "Examples of steady vortex rings of small cross-section in an ideal fluid," *J. Fluid Mech.* **51**, 119–135 (1972).
- <sup>27</sup>J. Norbury, "A family of steady vortex rings," *J. Fluid Mech.* **57**, 417–431 (1973).
- <sup>28</sup>M. Shusser and M. Gharib, "Energy and velocity of a forming vortex ring," *Phys. Fluids* **12**, 618–621 (2000a).
- <sup>29</sup>A. Glezer, "The formation of vortex rings," *Phys. Fluids* **31**, 3532–3542 (1988).
- <sup>30</sup>M. Shusser, M. Gharib, M. Rosenfeld, and K. Mohseni, "On the effect of pipe boundary layer growth on the formation of a laminar vortex ring generated by a piston/cylinder arrangement," *Theor. Comput. Fluid Dyn.* **15**, 303–316 (2002).
- <sup>31</sup>J. O. Dabiri and M. Gharib, "A revised slug model boundary layer correction for starting jet vorticity flux," *Theor. Comput. Fluid Dyn.* **17**, 293–295 (2004).
- <sup>32</sup>M. Shusser and M. Gharib, "A model for vortex ring formation in a starting buoyant plume," *J. Fluid Mech.* **416**, 173–185 (2000).
- <sup>33</sup>R. S. Heeg and N. Riley, "Simulations of the formation of an axisymmetric vortex ring," *J. Fluid Mech.* **339**, 199–211 (1997).
- <sup>34</sup>R. Von Mises, "Berechnung von ausfluß und überfallzahlen," *Ver. Dtsch. Ing. Z.* **61**, 469–474 (1917).
- <sup>35</sup>P. S. Krueger, "An over-pressure correction to the slug model for vortex ring circulation," *J. Fluid Mech.* **545**, 427–443 (2005).
- <sup>36</sup>X. K. Wang, B. Y. Su, Y. L. Li, and C. Wang, "Vortex formation and evolution process in an impulsively starting jet from long pipe," *Ocean Eng.* **176**, 134–143 (2019).
- <sup>37</sup>J. W. Zhu, G. Q. Zhang, L. Gao, and S. C. M. Yu, "The formation process of annular starting jets," *J. Fluid Mech.* **949**, A47 (2022).
- <sup>38</sup>L. Gao, X. Wang, S. C. M. Yu, and M. K. Chyu, "Development of the impulse and thrust for laminar starting jets with finite discharged volume," *J. Fluid Mech.* **902**, A27 (2020).
- <sup>39</sup>X. Zhang, J. Wang, and D. Wan, "CFD investigations of evolution and propulsion of low speed vortex ring," *Ocean Eng.* **195**, 106687 (2020).
- <sup>40</sup>P. S. Krueger, "Circulation of vortex rings formed from tube and orifice openings," in *Fluids Engineering Division Summer Meeting* (ASME, 2006), pp. 97–104.
- <sup>41</sup>P. S. Krueger, "Circulation and trajectories of vortex rings formed from tube and orifice openings," *Physica D* **237**, 2218–2222 (2008).
- <sup>42</sup>R. Holman, Y. Utturkar, R. Mittal, B. L. Smith, and L. Cattafesta, "Formation criterion for synthetic jets," *AIAA J.* **43**, 2110–2116 (2005).
- <sup>43</sup>P. S. Krueger and M. Gharib, "The significance of vortex ring formation to the impulse and thrust of a starting jet," *Phys. Fluids* **15**, 1271–1281 (2003).
- <sup>44</sup>H. F. Guo, L. Gao, and S. C. M. Yu, "Vortex formation in starting buoyant jets at moderate Richardson numbers," *Phys. Fluids* **32**, 117107 (2020).
- <sup>45</sup>L. Gao, H. F. Guo, and S. C. M. Yu, "A general definition of formation time for starting jets and forced plumes at low Richardson number," *J. Fluid Mech.* **886**, A6 (2020).
- <sup>46</sup>L. Gao and S. C. M. Yu, "Vortex ring formation in starting forced plumes with negative and positive buoyancy," *Phys. Fluids* **28**, 113601 (2016).
- <sup>47</sup>X. Zhou, Y. Xu, and W. Zhang, "Formation regimes of vortex rings in thermals," *J. Fluid Mech.* **885**, A44 (2020).
- <sup>48</sup>M. Rosenfeld, E. Rambod, and M. Gharib, "Circulation and formation number of laminar vortex rings," *J. Fluid Mech.* **376**, 297–318 (1998).
- <sup>49</sup>M. Rosenfeld, K. Katija, and J. O. Dabiri, "Circulation generation and vortex ring formation by conic nozzles," *J. Fluid Mech.* **131**, 091204 (2009).
- <sup>50</sup>M. Nitsche, "Scaling properties of vortex ring formation at a circular tube opening," *Phys. Fluids* **8**, 1848–1855 (1996).
- <sup>51</sup>T. T. Lim and T. B. Nickels, "Vortex rings," in *Fluid Vortices* (Springer, 1995), pp. 95–153.
- <sup>52</sup>D. Das and J. H. Arakeri, "Transition of unsteady velocity profiles with reverse flow," *J. Fluid Mech.* **374**, 251–283 (1998).
- <sup>53</sup>J. K. Vennard, *Elementary Fluid Mechanics* (Read Books Ltd, 2011).
- <sup>54</sup>K. Schlüter-Kuck and J. O. Dabiri, "Pressure evolution in the shear layer of forming vortex rings," *Phys. Rev. Fluids* **1**, 012501 (2016).
- <sup>55</sup>C. K. Batchelor and G. K. Batchelor, *An Introduction to Fluid Dynamics* (Cambridge University Press, 2000).